Reversible Multielectron Redox Activity of $LiNbV(PO_4)_3$ Anti-NASICON-Type Phosphate Towards Lithium and Sodium Intercalation

Ilia R. Cherkashchenko[ab], Rodion V. Panin[b], Artem D. Dembitsky[a], Daniil A. Novichkov[b], Dmitry A. Aksyonov[a], Evgeny V. Antipov[ba], Nellie R. Khasanova*[b]

[a] *Skolkovo Institute of Science and Technology, 143025, 3 Nobel Street, Moscow, Russia*

[b] *Department of Chemistry, Lomonosov Moscow State University, 119991, Leninskie Gory 1-3, Moscow, Russia.*

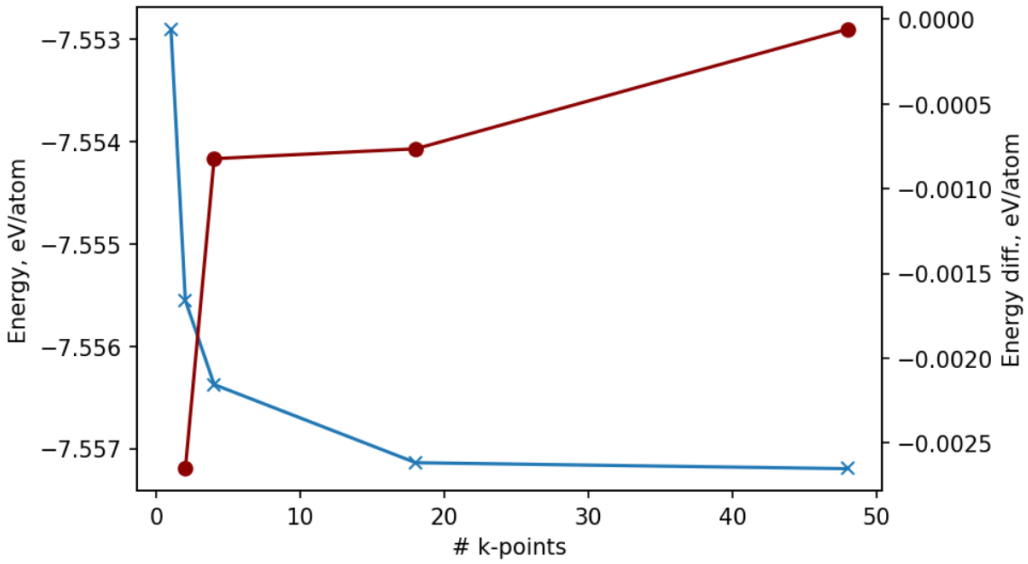

Fig. S1 The convergence of total energy as a function of k-mesh density.

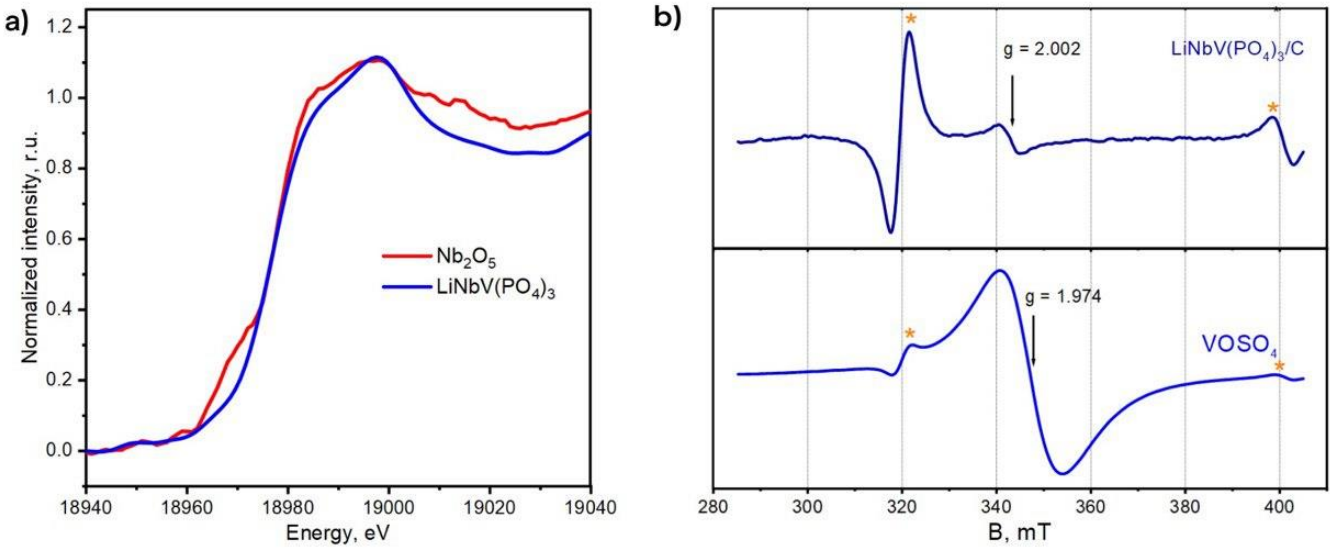

Fig. S2 (a) XANES spectra of initial $LiNbV(PO_4)_3$ with internal standard; (b) first-derivative EPR spectra of the $LiNbV(PO_4)_3$ and $VOSO_4$ reference samples, the asterisks show signals from internal ruby standard. The EPR spectrum of the sample $LiNbV(PO_4)_3$ demonstrates a weak signal centered at g = 2.002 (close to the free electron value g(e) = 2.0023) with the peak-to-peak linewidth of ca. 4 mT. This signal most likely originates from carbon, which is contained in the sample. No evidence for the presence of signal from paramagnetic V^{4+} ions has been detected. The signal from the $VOSO_4$ powder reference sample (g = 1.974) is shown for comparison.

Table S1 Atomic positions, ADPs and BVS for the $LiNbV(PO_4)_3$ structure.

Atom	Position	*x/a*	*y/b*	*z/c*	U_{iso}, Å^2	BVS
Li1*	*8d*	0.188	0.269	0.291	0.04	1.03
Nb1/V1**	*8d*	0.3856(3)	0.2602(6)	0.4855(6)	0.011(1)	Nb 5.21/V 3.30
P1	*4c*	0	0.462(2)	0.25	0.032(3)	5.06
P2	*8d*	0.355(1)	0.371(2)	0.084(1)	0.032(3)	4.96
O1	*8d*	0.342(2)	0.546(2)	0.060(2)	0.007(2)	2.38
O2	*8d*	0.075(1)	0.355(2)	0.160(2)	0.007(2)	2.41
O3	*8d*	0.271(1)	0.311(2)	–0.035(2)	0.007(2)	2.00
O4	*8d*	–0.058(2)	0.586(2)	0.150(2)	0.007(2)	1.96
O5	*8d*	0.463(1)	0.326(2)	0.003(2)	0.007(2)	2.24
O6	*8d*	0.343(2)	0.340(2)	0.258(1)	0.007(2)	1.71

* the occupancy 0.5.

** 0.5 Nb + 0.5 V.

Table S2 Selected interatomic distances for $LiNbV(PO_4)_3$.

Bond	d, Å	Bond	d, Å
Nb1/V1 – O1	1.87(2)	P2 – O1	1.53(2)
Nb1/V1 – O2	1.87(2)	P2 – O3	1.54(2)
Nb1/V1 – O3	2.01(2)	P2 – O5	1.53(2)
Nb1/V1 – O4	2.03(2)	P2 – O6	1.55(1)
Nb1/V1 – O5	1.92(2)	Li1 – O2	1.93(2)
Nb1/V1 – O6	2.16(1)	Li1 – O3	1.74(2)
P1 – O2	2×1.52(2)	Li1 – O5	2.73(2)
P1 – O4	2×1.54(2)	Li1 – O6	2.00(2)

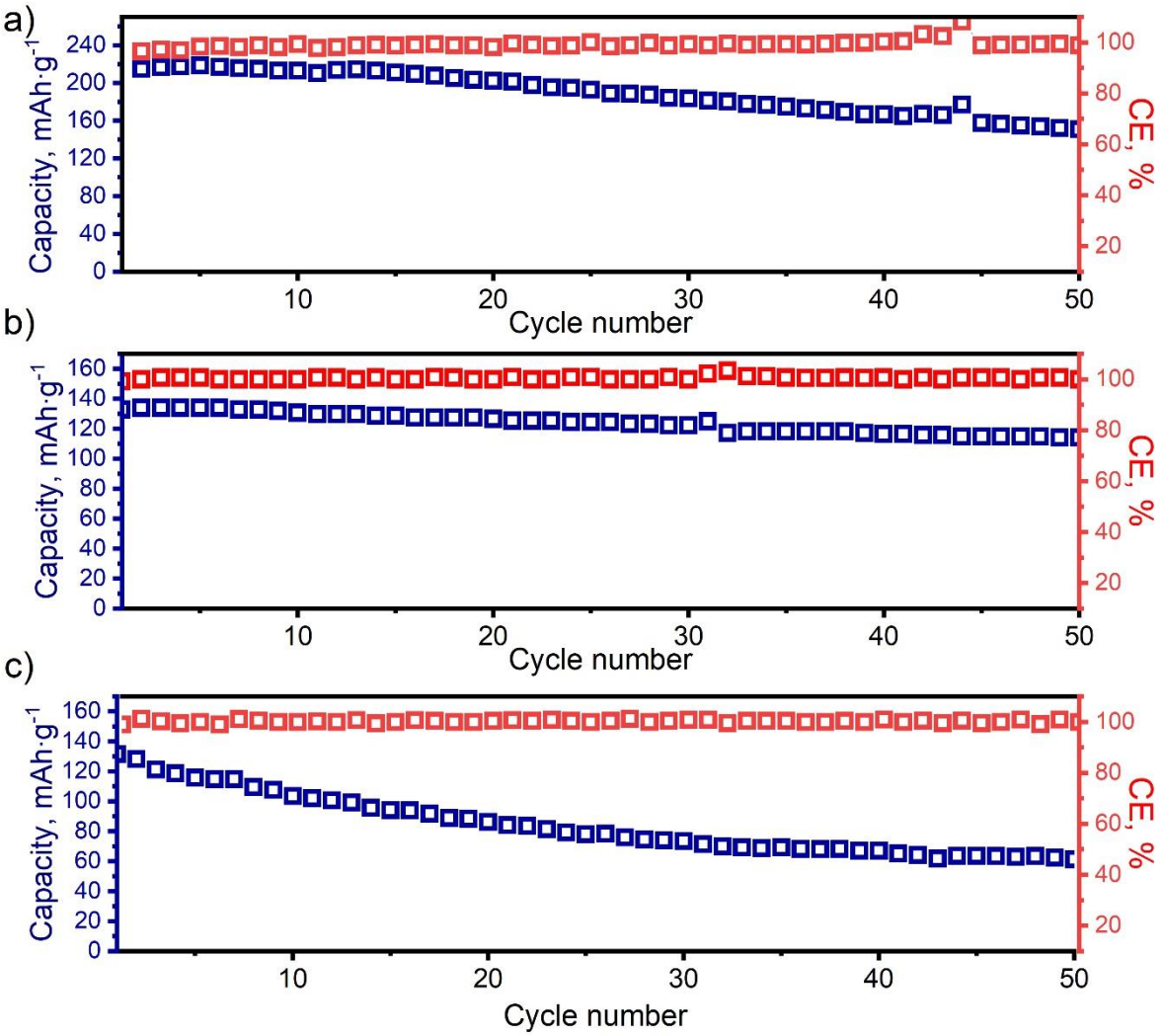

Fig. S3 Results of galvanostatic cycling for $LiNbV(PO_4)_3$ in the Li half-cell at 1C rate within 1.15-4.1 V (a), and 1.5-4.1 V (b) potential ranges; and in the Na half-cell at 0.2C rate between 0.9-3.0 V (c).

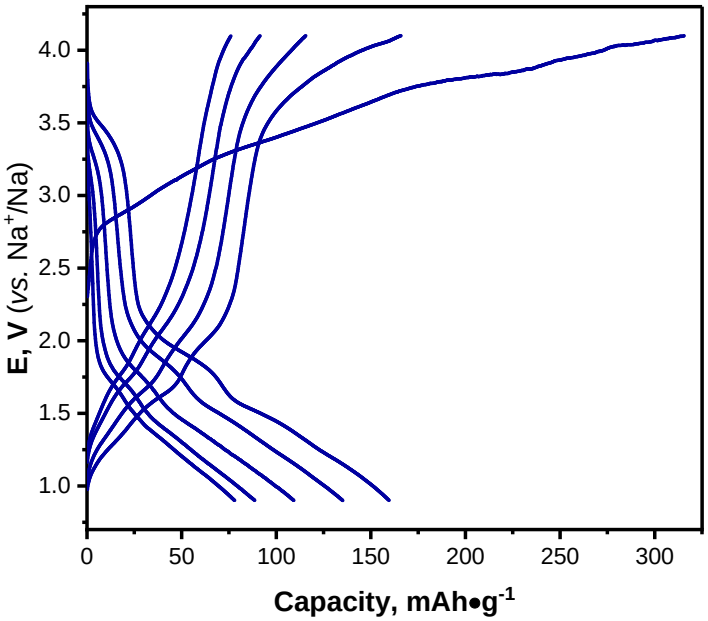

Fig. S4 Galvanostatic curves of $LiNbV(PO_4)_3$ in the Na half-cell at C/10 rate in the 0.9-4.1 V potential range.

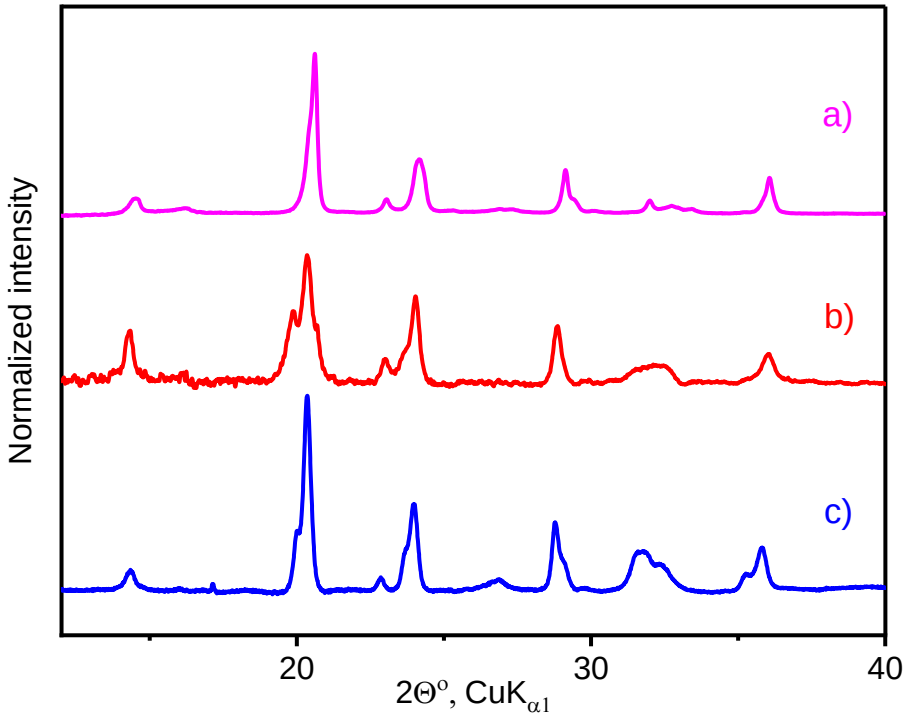

Fig. S5 *Ex situ* XRD patterns of the pristine $LiNbV(PO_4)_3$ (a), lithiated "$Li_4NbV(PO_4)_3$" (b) and sodiated "$Na_3LiNbV(PO_4)_3$" (c) electrode materials.

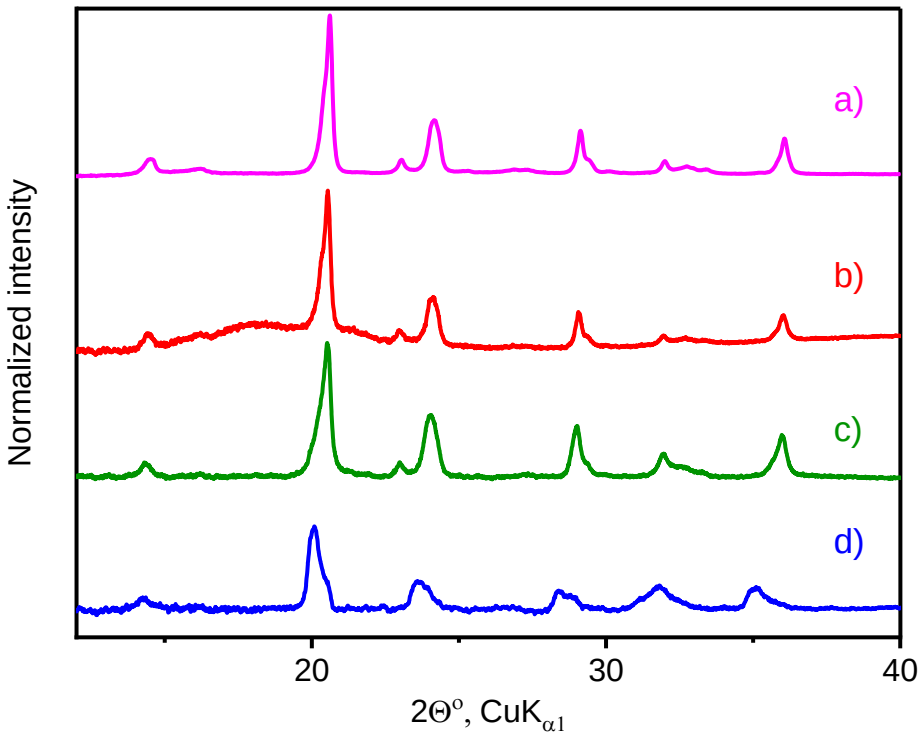

Fig. S6 *Ex situ* XRD patterns of the pristine $LiNbV(PO_4)_3$ (a), delithiated "$Li_0NbV(PO_4)_3$" (b) and sodiated "$NaLiNbV(PO_4)_3$" (c) "$Na_4NbV(PO_4)_3$" (d) electrode materials.

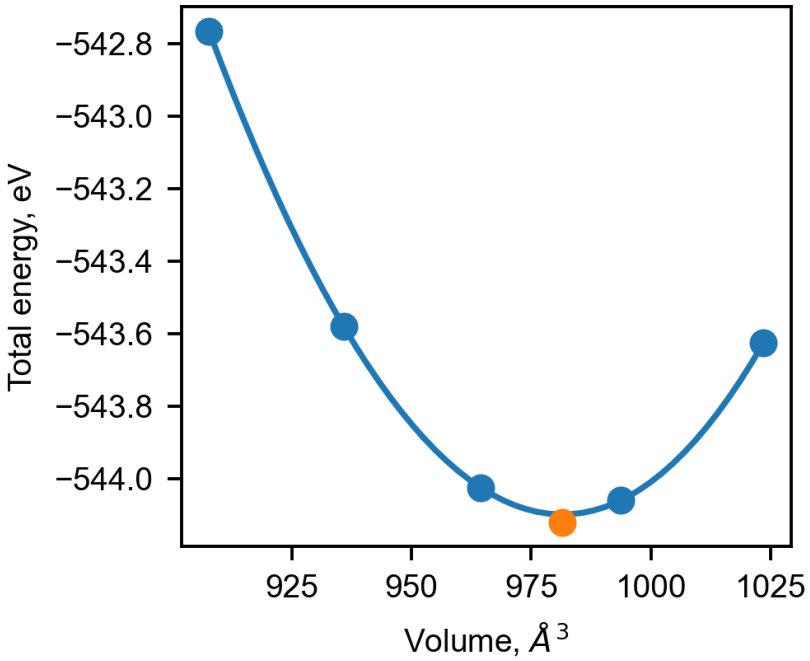

Fig. S7 Equation of state for the $NaNbV(PO_4)_3$ obtained with PBE+U calculations. The overestimation of the parameters is due to the PBE functional used and may be caused a slight difference in composition between the theoretical model and the experimental sample. This could be due to Li residual present in the $NbV(PO_4)_3$ structure after electrochemical delithiation.

Table S3 Comparison of the calculated DFT PBE+U optimized lattice constants with the Le Bail fitting experimental.

Lattice parameters	Exp	PBE+U	diff, %
a, Å	8.6227	8.84	2.52
b, Å	8.7766	8.92	1.63
c, Å	12.1468	12.44	2.41
V, Å^3	919.2454	981.37	6.76

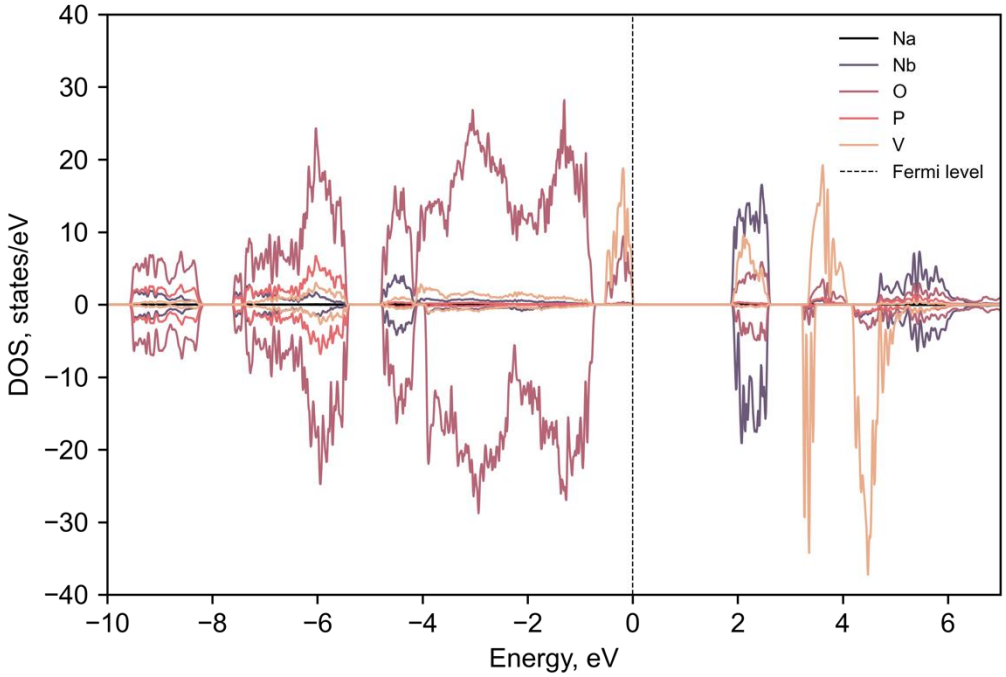

Fig. S8 The atom-projected $NaNbV(PO_4)_3$ density of states (DOS) for ferromagnetic state calculated with GGA PBE+U. DOS was smoothed using Gaussian filtering and shifted to set Fermi energy (valence band maximum) at zero energy. The total energy of the antiferromagnetic state is 0.6 meV/atom higher than that of the ferromagnetic state.

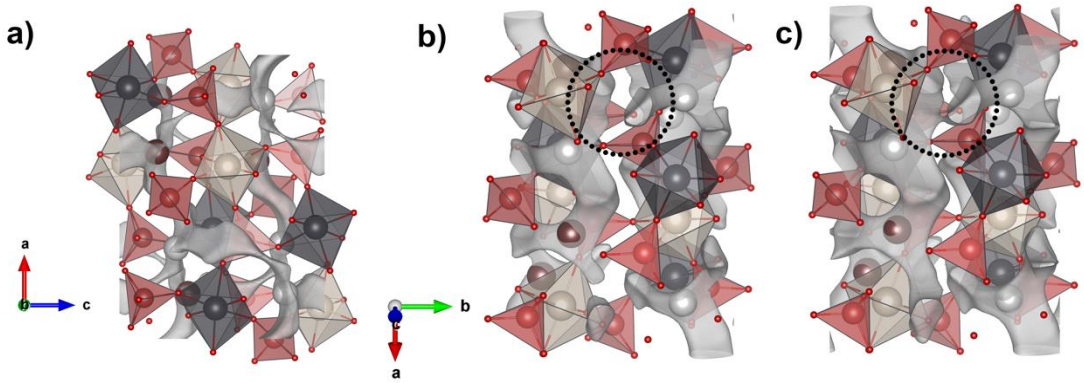

Fig. S9 BVSE calculated Na^+ diffusion networks. a-b) 2D percolation in *bc*-plane (isosurface level is 1.2 eV above the minimum), c) 3D percolation (isosurface level is 1.8 eV above the minimum), the bottleneck is highlighted with a dashed circle. The calculations were performed using *bvlain* python library.[1]

Table S4 The studied Na^+ vacancy and interstitial migration hops. Each jump is described by five numbers – first two numbers correspond to the source and target ion positions in the unit cell, while the rest three numbers correspond to the offset translational vector of the target positions.

#	jump	distance, Å	barrier, eV	comments
1	3 0 1 0 0	4.89	0.49	vacancy
2	0 3 0 0 0	4.97	0.48	vacancy
3	1 3 0 0 0	5.16	0.40	vacancy
4	3 1 0 1 0	4.66	0.73	vacancy
5	2 3 0 0 1	4.07	0.20	vacancy
6	0 4 0 0 0	4.64	0.51	interstitial
7	1 4 0 0 0	4.49	0.57	interstitial
8	1 6 0 0 0	4.3	0.72	interstitial
9	2 6 0 1 0	4.89	0.53	interstitial

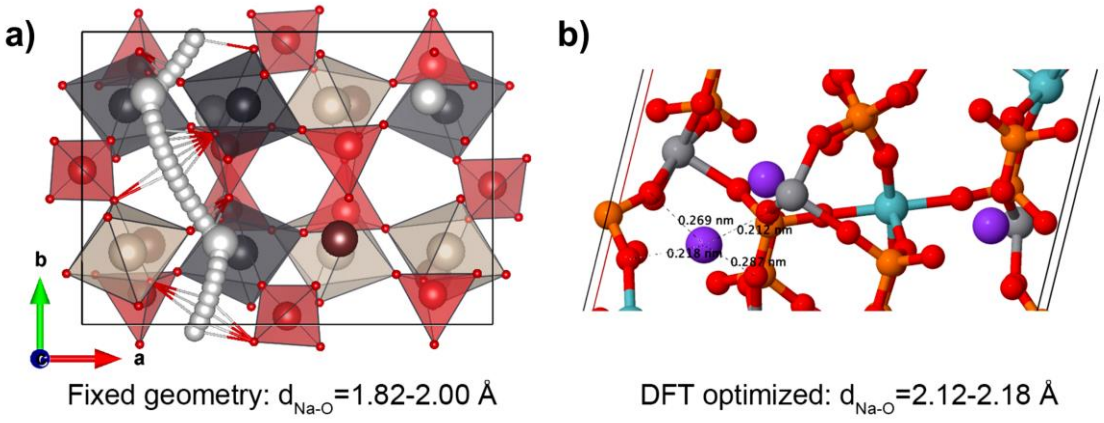

Fig. S10 Comparison of the coordination of the migrating Na ion along the b-axis. a) Fixed geometry, only Na-O bonds shorter than 2.0 Å are shown. b) DFT-NEB optimized geometry; saddle point of the migration trajectory.

Section S1. DFT calculations: analysis of structural descriptors

To understand which structural features (descriptors) have the greatest impact on activation barriers, we examined the correlation between the barriers and changes in local geometry along the migration pathway. According to obtained results, the analysis of local structural features along the migration pathway for anti-NASICON structured $NaNbV(PO_4)_3$ adequately characterizes changes in the activation barrier and allows for a quantitative description, at least within the context of this compound. This is important because it is widely accepted that geometric descriptors can only be used qualitatively to distinguish between good and poor ionic conductors.

For that, we calculated the geometric characteristics of the Voronoi polyhedra (such as area, volume, face distance, maximum/minimum solid angle associated with the faces of the Voronoi polehedron, and coordination number) corresponding to the Na^+ ions at the minimum and maximum energy states along the elementary migration hop and the absolute difference between these descriptors. Additionally, we included the curvature of the trajectory in the feature list, calculated as the ratio of the relaxed curved pathway length to the straight-line distance between the end points of the pathway. The calculated correlation matrices for the selected descriptors and activation barrier are shown in Fig. S11-S12 (comments to the figures in the Table S5). According to the calculations, there is a strong correlation between the difference in the maximum solid angle at minimum and maximum energy states (0.84). This suggests that this single feature can effectively explain the variation in activation barriers. Among the studied absolute quantities at the maximum energy state, the coordination number of Na^+ has a stronger effect on the activation barrier (0.78, Fig. S11), than the differential values. Another important descriptor is the volume change of the Voronoi polyhedron along the trajectory (correlation is 0.68). We reveal that features associated with the local heterogeneities along the conductive channel might be more informative than the absolute characteristics of the migration pathway, such as migration length (0.31 correlation) or the coordination of the saddle point.

We also note that the curvature of the trajectory exhibits a higher correlation with E_a in comparison to the length of the pathway which might be a sign that the curvature feature latently stores the information about the potential energy surface changes within the conductive channel. Overall, the analysis of the local structural features along the migration pathway adequately characterizes the changes in the activation barrier, enabling quantitative description, at least within the framework of the considered compound. This is noteworthy since it is widely accepted that geometrical descriptors are only suitable for qualitatively differentiating between high and poor ionic conductors.[2] However, we note that these features are calculated for the DFT optimized trajectory, hence these can be used only for the analysis but not for the prediction of the activation barriers.

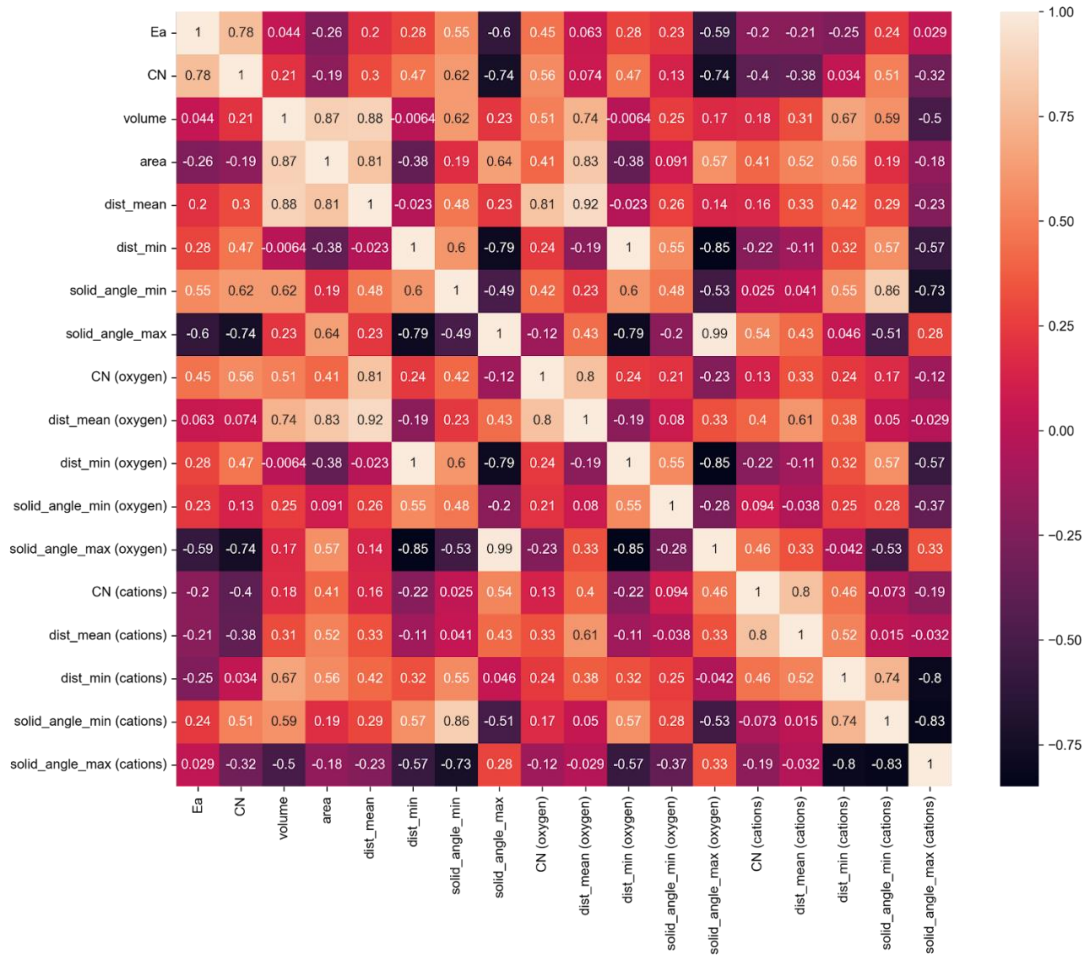

Fig. S11 Correlation matrix of the calculated activation barriers and the geometrical descriptors at the maximum energy states along the Na-Na migration pathway derived via Voronoi partitioning. Note that the quantities used for calculating the correlation coefficients are the absolute values at the maximum energy state along the migration trajectory (in comparison to the Fig. S12, where the absolute difference of the quantities at the maximum and minimum energy states were used).

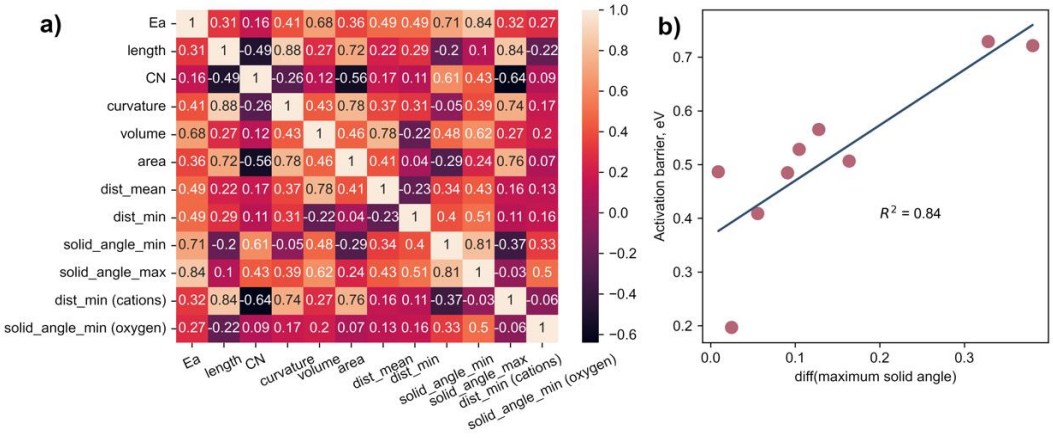

Fig.S12 a) Correlation matrix of the calculated activation barriers and the changes in geometrical descriptors of the minimum and maximum energy states along the Na-Na migration pathway derived via Voronoi partitioning as implemented in *pymatgen*[1] b) Migration barrier as a function of differential maximum solid angle. Note that the quantities used for calculating the correlation coefficients are the absolute difference (not absolute values) between two descriptors calculated at minimum and maximum energy states along the migration trajectory (excluding length and curvature features).

Table S5 Description of Voronoi partitioning derived features. The features were collected for the mobile ion at the position corresponding to the minimum and maximum energy states along the optimized migration trajectory. Voronoi partitioning was carried out for the crystal structure as is, for cation sublattice and for the sublattice containing oxygen and sodium.

Feature	Description
volume	Volume of the Voronoi polyhedron constructed around the mobile ion
length	Distance between the start and end position of the migration trajectory
CN	Effective coordination number of the mobile ion
curvature	Length of the optimized migration pathway divided by the distance between the start and end position of the migration trajectory
dist_mean (av_dist in the main text)	Average distance between the mobile ion and its coordination
dist_min	Minimum distance between the mobile ion and its coordination
area	Total area of the Voronoi polyhedron calculated as the sum of areas of Voronoi polyhedron faces
Solid angle	Solid angle corresponding to a face of the Voronoi polyhedron

References

1 S.P. Ong, W.D. Richards, A. Jain, G. Hautier, M. Kocher, S. Cholia, D. Gunter, V.L. Chevrier, K.A. Persson and G. Ceder, *Comput. Mater.Sci.*, 2013, **68**, 314–319.

2 D. A Aksyonov, A. O. Boev, S. S. Fedotov and A. M. Abakumov, *Solid State Ion.*, 2023, **393**, 116170.